2.6 THREE DIMENSIONAL ATOM PROBE TOMOGRAPHY OF 14YW AND 14YWT NEUTRON IRRADIATED AT 500ºC TO 21.2 DPA—D.J. Edwards, K. Kruska, J. Wang, R. J. Kurtz (Pacific Northwest National Laboratory), G.R. Odette, T. Yamamoto and Y. Wu (University of California-Santa Barbara)

OBJECTIVE

The aim of this study is to characterize the nano-oxide dispersion and precipitates in neutron irradiated ferritic alloys 14YWT and 14YW by atom probe tomography.

SUMMARY

Work has progressed on the characterization of two ferritic alloys, 14YW and 14YWT, irradiated in the JP27 experiment in the High Flux Isotope Reactor as part of the In-situ Helium Injection (ISHI) experiments. While much of the work has focused on high resolution analytical TEM of the bubble and dislocation structures formed during neutron irradiation, this TEM analysis has not been able to effectively characterize the nano-oxide particles present in 14YWT, which are usually less than 2 nm in size. To investigate microstructural features at this scale in a statistically meaningful manner, 3D-APT has been initiated to probe the oxide dispersion in the 14YWT. For comparative purposes, the 14YW alloy is also examined, however, the oxide dispersion is noticeably coarser due to the lack of titanium, and it is better characterized using TEM. APT of the 14YWT alloy revealed that significant precipitation of Mn-rich phases had occurred, as well as the formation of a Cr-rich α'-type phase at a composition that appears to contain less than the expected 85% Cr.

PROGRESS AND STATUS

Introduction

Oxide-dispersed strengthened (ODS) ferritic alloys, nanostructured ferritic alloys (NFA) and reduced activation ferritic/martensitic (RAFM) steels are currently considered the most viable candidates for structural materials for next step plasma devices]1,2]. This is due in large part to their excellent high-temperature mechanical properties and high swelling-resistance under neutron irradiation [1,2]. However, transmutation might cause significant degradation of these properties due to the large levels of helium produced during device operation. Up to 2,000 appm of helium could be produced, which is known to lead to helium bubble formation, promoting embrittlement, void swelling, and potentially enhanced irradiation creep. Understanding how helium accumulates at and interacts with various microstructural features such as grain boundaries, particle interfaces, and dislocations of various types can help to design more helium tolerant microstructures.

The following report summarizes a new set of 3D-atom probe tomography analyses conducted on two nanostructured ferritic alloys, 14YWT and 14YW, both oxide dispersion alloys based on a nominal 14Cr composition with only a few tenths of a percent of yttrium present in the form of oxide particles. The main difference between these alloys is the lack of titanium in the 14YW, the absence of which leads to a much coarser distribution of particles than is found in the 14YWT. Both of these alloys have been studied using analytical TEM, and the results of these studies have been reported in a prior semi-annual report by Jung et al [3].

Experimental Procedure

3-mm TEM discs of 14YWT and 14YW were neutron irradiated in the JP27 experiment to a dose of 21.2 dpa at 500°C in the High Flux Isotope Reactor (HFIR) at Oak Ridge National Laboratory (ORNL). The nominal compositions in the as-irradiated state as determined by EDS are provided in Table 1. While the compositions are similar to the unirradiated state, note that the tungsten experiences a significant degree of transmutation in the highly thermalized neutron environment of HFIR, leading to some of the W being

transmuted into Os and Re. In addition, Fe and Cr both undergo transmutation to Mn, not only producing a few tenths weight percent of Mn, but also producing strong Mn x-rays at 5.9 and 6.5 keV via the decay of ^{55}Fe to ^{54}Mn, which needs to be accounted for in the EDS analysis from bulk samples. EDS analysis of a FIB lamella, which has virtually no detectable radioactivity because of the small volume, revealed the Mn concentration in both alloys was approximately 0.4 wt%.

A 4 µm NiAl coating used for the ISHI was applied to one side of a 3-mm TEM disc, which allows 3D-APT needles to be extracted from either side of the TEM disc to explore the impact of neutron irradiation with or without concurrent helium injection. At 21.2 dpa, the NiAl coating produces a He concentration of about 1,230 appm in the ferritic matrix extending to a depth of ~6 µm below the coating. 3D-APT needles were prepared using an FEI Quanta 3D from the neutron irradiated side of the disc. The surface of the disc was heavily oxidized, so the surface was lightly ground and then given a short electropolish using a 5% perchloric/95% methanol solution cooled to -60ºC. The electropolishing allowed the grain structure to be imaged in order to extract APT needles from the grain interiors or grain boundary regions.

The APT analysis was conducted using the LEAP® 4000 XHR instrument in the Environmental Molecular Science Laboratory User facility. Multiple needles were run at 44K using a laser wavelength of 355 nm, a pulse energy of 60 pJ, and a pulse frequency of 125-250 kHz.

Table 1. Composition of Ferritic alloys After Neutron Irradiation

Alloy	Composition (wt.%) with Fe balance											
	Al	**Si**	**Ti**	**Cr**	**Mn***	**Fe**	**Ni**	**Y**	**Mo**	**W**	**Re**	**Os**
14YW	1.61	0.79	0.00	13.70	~0.4	78.97	0.09	0.05	0.04	1.97	0.08	0.51
14YWT	0.82	0.22	0.41	13.76	~0.4	79.25	0.09	0.13	0.07	2.04	0.21	0.54

* *Mn levels are artificially high due to a contribution from radioactive decay, EDS analysis of a FIB lamella from each irradiated alloy showed around 0.4 wt% Mn.*

Results

The reconstruction of the APT data revealed a complicated microstructure. A thorough quantitative analysis is in progress, so only highlights will be presented here. Two needles from the 14YWT disc revealed a varying microstructure dependent on the lift-out location. One needle had relatively large Cr-O particles and smaller Ti-Cr-O particles. The 3D-APT dataset in Figure 1 shows the ion maps for the Fe, Y, CrO, TiO and Mn. This dataset revealed a number of different phases, including four large inclusions and a host of much smaller precipitates, some of which were found to be Mn-rich particles containing significant levels of Cr, Ti, Si, N and O. The compositions of the four large particles, as derived from the APT dataset, are provided in Table 2. Figure 2 shows iso-concentration surface plots for the various precipitates in the dataset, clearly demonstrating a high density of small particles interspersed among the larger particles. The Mn ion map in Figure 2(b) shows the Mn clustering, revealing both discrete particles as well as segregation around the outer surfaces of some of the larger particles. The summed composition of these clusters indicates approximately 4.4 at% Mn, 4.6 at% Ti, 22.6 at% Cr, 26 at% O, and Si and N at around 1 to 1.4 at%. Analysis of this sample also revealed clusters of Ti-Y-O of varying compositions, but requires further analysis to confirm the actual compositions. Analysis of the Cr-rich alpha prime is ongoing. Another dataset from the 14YWT disc has been acquired and will be summarized in future reports.

Recently acquired APT data from the grain interiors of irradiated 14YW show no large particles as found in the first needle for 14YWT. The Mn distribution has not yet been characterized, but the alpha prime distribution has been analyzed as shown in Figure 3 for two different needles. The alpha prime is easily visible as small clusters of Cr, and there is minor variation between the needles in terms of spatial homogeneity. The density of alpha prime, based on the 25 at% iso-concentration surface plots, varies from ~3 to 6 x 10^{23} m^{-3}, with a mean size of around ~3 ± 1 nm. The proxigrams for each needle reveal

Figure 1. An ion map shows the elemental distribution within this particular needle. Four large particles are highlighted for subsequent examination. Analysis revealed a grain boundary close to particles #2 and #3. The grain boundary only shows slight enrichment in C, but no major segregation of other alloying elements. The bulk composition of each overall particle is listed in Table 2, but a more complete analysis revealed particle #4 exhibited a Ti(Cr)N core with a Ti(Cr)O shell.

Table 2. Compositions (at%) of the Large Particles from Figure 1

	Si	N	Ti	Cr	Y	O
Particle #1	0.35	0.23	2.71	36.01	0.51	45.92
Particle #2	3.28	3.36	12.21	14.18	7.58	26.49
Particle #3	0.62	0.34	2.75	32.74	0.11	39.97
Particle #4	2.03	8.2	17.09	19.88	0.72	21.2

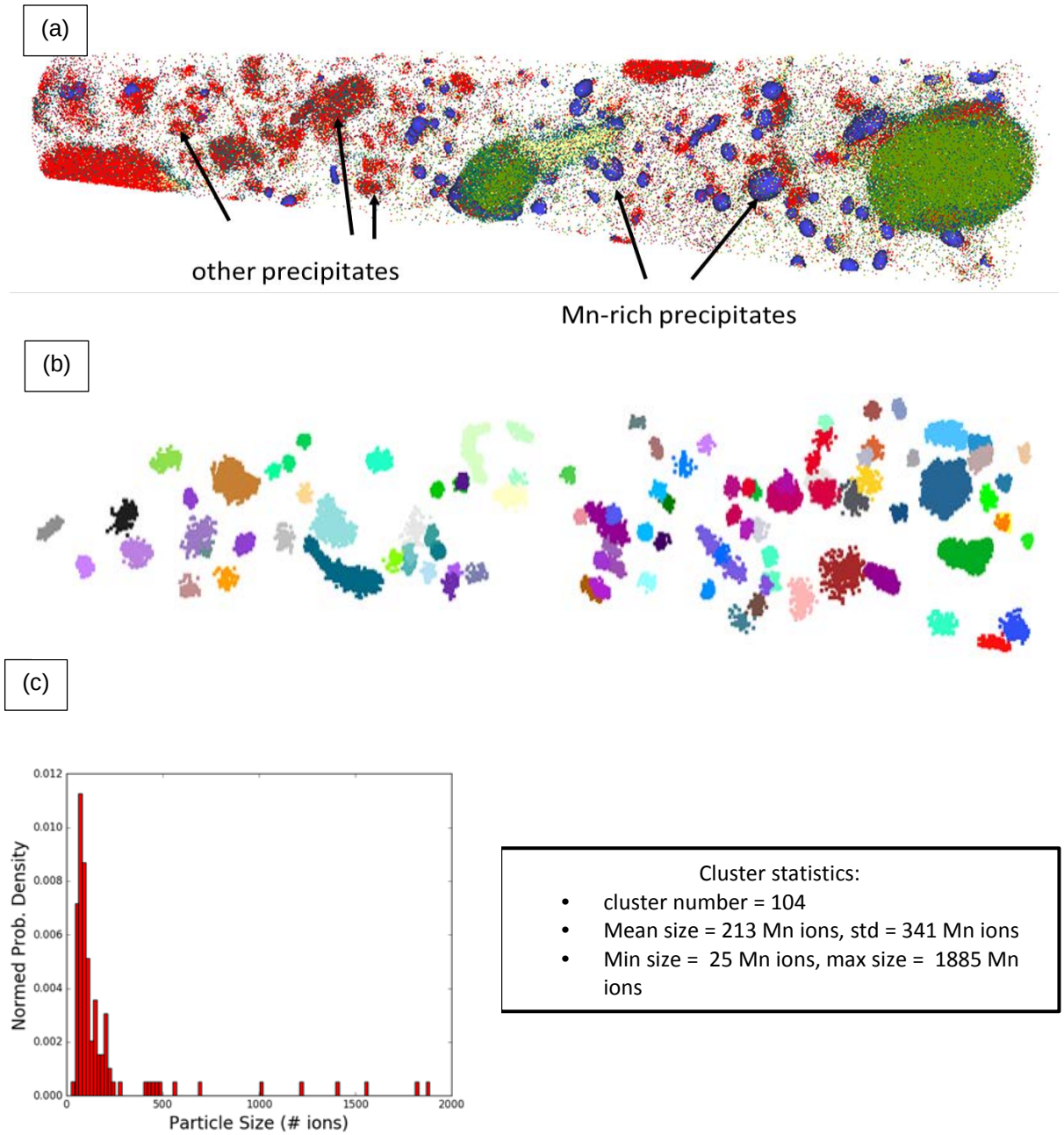

Figure 2. Iso-concentration plots reveal a number of different particles of varying sizes. The blue particles in (a) were found to be Mn-rich particles with significant levels of Cr, O, Si, N and Ti. The Mn only map is provided in (b), showing that discrete Mn-rich particles are present, but there is also some association between the Mn and the outside of the larger particles identified in Figure 1. The Mn cluster size distribution shown in (c) reveals that Mn-rich clusters follow a narrow distribution and contains ~200 Mn ions in average (roughly ~2.5 nm, given the measured Mn concentration is ~3-4 at.% inside clusters), with a few precipitates extending up to nearly 10 nm. The measured statistics for the distribution are provided in the inset table.

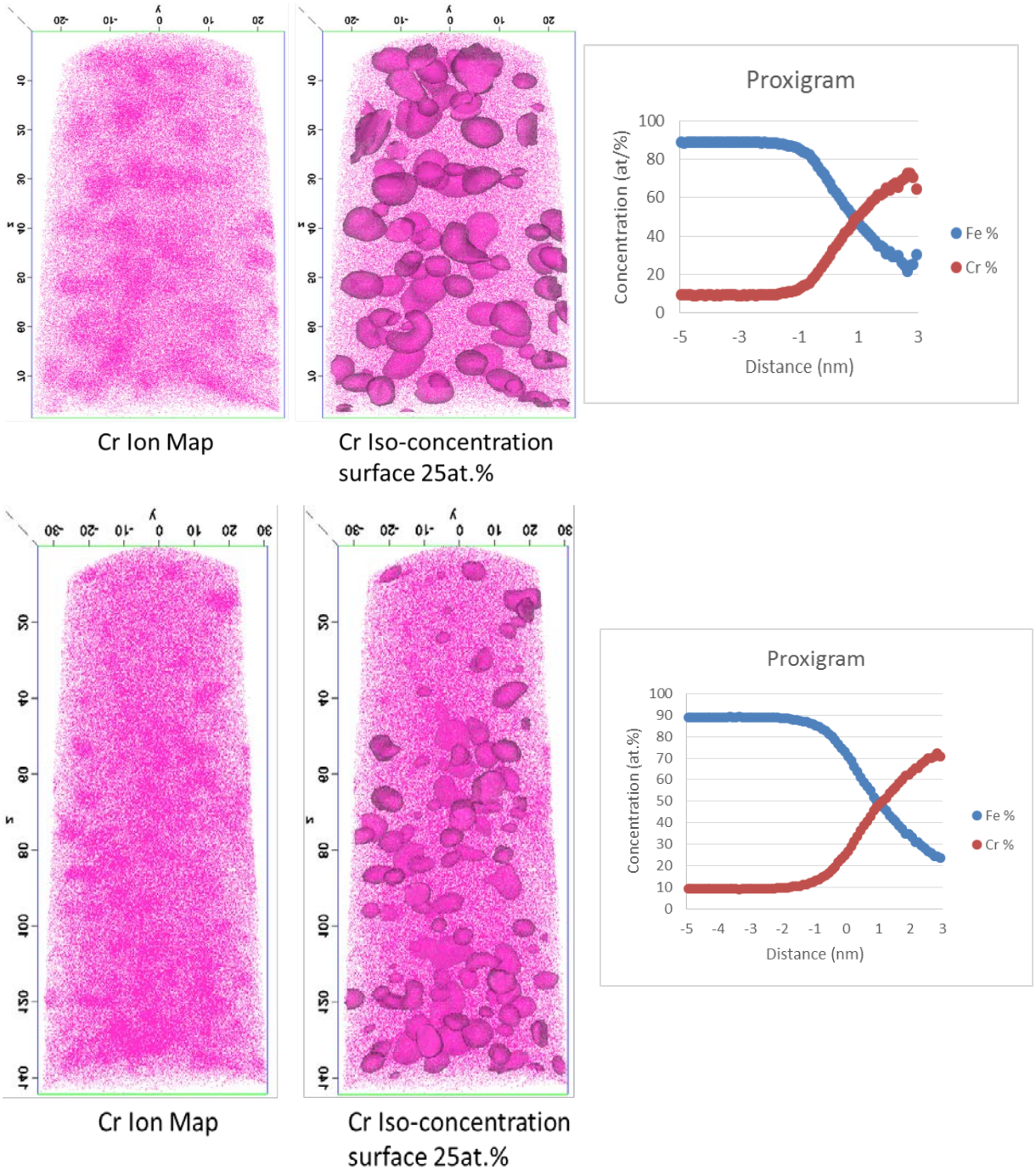

Figure 3. Cr ion maps, iso-concentration plots and proxigrams are provided for two different needles, revealing a high density of alpha prime clusters in a somewhat varying spatial distribution.

the alpha prime Cr level reaches a max of around 70 at%. The nano-oxides of the 14YW are coarser than found in the 14YWT, so only a few of the smaller particles were actually captured in these two datasets. TEM analysis will be needed to more fully characterize the oxide particle distribution in this particular alloy in combination with the results of the APT analysis. In addition, further analysis will probe the clustering of other elements such as Mn to complete the picture of elemental evolution for these two alloys.

Future Work

Additional analyses are planned for the APT data to achieve a consistent comparative analysis between the microstructures of these two irradiated alloys. In addition, work is planned to explore correlative high resolution TEM/STEM on APT needles prior to an APT run. The aim will be to document the distribution of helium bubbles and cavities, dislocation structures, precipitates and elemental segregation as can be measured in the aberration corrected JEOL ARM200CF. Subsequently, these needles will be run in the LEAP 4000 with the hope to fully interrogating the microstructure over a range of length scales with two different high-resolution techniques.

Acknowledgements

This research was supported by Office of Fusion Energy Sciences, U.S. Department of Energy (DOE) under Contract DE-AC05-76RL01830. APT was performed under a general user proposal at the Environmental Molecular Sciences Laboratory (EMSL), a national scientific user facility located at PNNL.

References

[1] [1] G.R. Odette, M.J. Alinger, and B.D. Wirth, Annu. Rev. Mater. Res. 38 (2008) 471.

[2] R.J. Kurtz, A. Alamo, E. Lucon, Q. Huang, S. Jitsukawa, A. Kimura, R.L. Klueh, G.R. Odette, C. Petersen, M.A. Sokolov, P. Spätig, J.W. Rensman, J. Nucl. Mater. 386-388 (2009) 411.

[3] H.J. Jung, D. J. Edwards, B. Yao, R. J. Kurtz, G. R. Odette, T. Yamamoto , Fusion Reactor Materials Program 56 (2014) 19